ADVANCING EARTH AND SPACE SCIENCE

Geophysical Research Letters

RESEARCH ARTICLE

Future Redistribution of North Atlantic Tropical Cyclone Risk in Two Contrasting CMIP6 Scenarios

Ratnaksha Lele[1], **Adam H. Sobel**[1,2], **Chia-Ying Lee**[1], **Suzana J. Camargo**[1,3], **Michael K. Tippett**[2], **Patrick Kelly**[4], **Ted Amdur**[5], **Radovan Drinka**[5]

[1]Lamont-Doherty Earth Observatory, Columbia University, Palisades, NY [2]Department of Applied Physics and Applied Mathematics, Columbia University, New York, NY [3]Columbia Climate School, Columbia University, New York, NY [4]Aon Climate Risk Advisory, USA [5]Aon Impact Forecasting, Chicago, IL

Key Points:

- Statistical-dynamical downscaling shows the future redistribution of North Atlantic TC activity under CMIP6 low and high forcing scenarios
- Regional North Atlantic TC trends show comparable risk under both scenarios despite different warming levels
- Future regional North Atlantic TC activity is more sensitive to SST warming pattern than to its global mean change

Correspondence to:
Ratnaksha Lele
rlele@ldeo.columbia.edu

Citation:
Your citation here.

Abstract

We analyze North Atlantic Tropical Cyclone (TC) activity using the Columbia HAZard (CHAZ) model to downscale 12 models from CMIP6 under the SSP1-2.6 and SSP5-8.5 scenarios — representing low and high radiative forcing, respectively. Despite greater warming under SSP5-8.5, basin-wide North Atlantic TC frequency is not consistently higher than under SSP1-2.6, contrasting the global-mean response. Landfalling TC frequency increases along the Southeastern U.S. and declines along the Gulf under both SSPs, a contrast that persists throughout the 21st century. Both TC genesis and steering flow changes contribute to this contrast, and appear consistent with projected El Niño-like shifts in the tropical Pacific mean state, influencing both Atlantic potential intensity and vertical wind shear variability. These results emphasize the sensitivity of regional TC activity to the spatial pattern of surface warming over its global-mean change, and the significance of the contention around projected trends in the tropical Pacific, in particular.

Plain Language Summary

Tropical cyclones (TCs) cause major damage along the U.S. coastline, and understanding how TC risk may change in the future is an important consideration for climate adaptation. We used a tropical cyclone risk modeling framework driven by projections from 12 global climate models to examine how storm landfalls in the North Atlantic might change under low and high greenhouse gas (GHG) emission scenarios. The results show a clear regional contrast: storms become more frequent along the Southeastern U.S. coast but less frequent along the Gulf Coast, including Texas. This pattern appears in both future climate scenarios and becomes stronger later in the 21st century. The Atlantic TC changes are linked to patterns of change in oceanic and atmospheric conditions that resemble those often seen during El Niño events. These environmental changes are consistent with trends towards a more El Niño-like mean state, which is not present in historical observations. Our results suggest that changes in regional TC risk depend less on the overall amount of global warming than on its spatial pattern, and that future changes in the pattern of tropical Pacific climate change are particularly important to North Atlantic TC activity and U.S. TC risk.

1. Introduction

Tropical cyclones (TCs) are among the most damaging natural hazards on Earth, producing widespread societal and economic impacts globally, especially in coastal regions. Understanding the present-day TC hazard risk and how it may evolve under anthropogenic climate change remains a key challenge for the scientific community (Broccoli & Manabe, 1990; Bengtsson et al., 1996; Landsea et al., 1999; Knutson et al., 2010; Sobel et al., 2016; Walsh et al., 2016; Knutson et al., 2020; Camargo et al., 2023). Along with analysis of the observational record, process-based understanding is essential to meeting this challenge.

TC activity is controlled by a combination of environmental factors including potential intensity (PI), vertical wind shear, mid-tropospheric humidity, and large-scale vorticity (Gray, 1968, 1984; Emanuel, 1987; Camargo, Sobel, et al., 2007; Sobel et al., 2016), which in turn are themselves shaped by large-scale circulation patterns and sea surface temperature (SST) distributions. Changes in the location of preferred genesis regions can modify track distributions (B. Wang & Chan, 2002; Camargo, Robertson, et al., 2007; Daloz et al., 2015), while alterations in large-scale steering flows can shift storm translation direction and speed (Chan, 2005; Colbert et al., 2013). These dynamical responses can lead to substantial regional changes in TC hazard by redistributing TC activity within basins (Jones & Thorncroft, 1998; Saunders et al., 2000; Murakami & Wang, 2010; Yokoi et al., 2013; Nakamura et al., 2017).

Assessments of tropical cyclones' response to climate change have tended to focus on global-scale aspects. At global scales, for example, there is relatively high confidence that warming intensifies the strongest storms (e.g., Knutson et al., 2015; Yoshida et al., 2017; Knutson et al., 2020), while on the other hand projections of TC frequency remain highly uncertain (Knutson et al., 2010; Walsh et al., 2016; K. A. Emanuel, 2013; Zhao et al., 2026; Vecchi et al., 2019; Sobel et al., 2021; Camargo et al., 2023; Chavas et al., 2025). A focus on global-scale changes could potentially bias regional hazard and risk assessments, if the global-scale changes are assumed to apply directly at local scales (e.g., Jewson, 2024). Recent studies show evidence that TC activity responds to the spatial pattern of surface warming rather than to its global mean (e.g., Sobel et al., 2023; J. Lin et al., 2025). PI responds to SST measured relative to the tropical mean more than to spatially uniform increases in absolute SST (Vecchi & Soden, 2007a; Ramsay & Sobel, 2011), so that Atlantic TC activity is only weakly constrained by the level of global-mean warming (Camargo et al., 2013; Sobel et al., 2016). Less well examined is how that dependence influences regional TC risk. Here we show that for TCs, changes on basin and sub-basin scales can be larger or smaller than those at global scales, and that the pattern of surface warming shapes not only the basin-wide response but the distribution of landfall risk along the U.S. coastline.

We use the Columbia HAZard (CHAZ) model (Lee et al., 2018), a statistical–dynamical framework which has been previously used to downscale simulations from Coupled Model Intercomparison Project (CMIP) simulations to project changes in global and regional TC activity (e.g., Lee et al., 2020; Fosu et al., 2024), as well as to economic losses from landfalling TCs (Meiler et al., 2022; Baldwin et al., 2023). CHAZ is one of a class of statistical–dynamical downscaling models (e.g., K. A. Emanuel et al., 2008; Lee et al., 2018; Bloemendaal et al., 2020; Jing & Lin, 2020), that synthesize large catalogs of physically consistent synthetic TCs using environmental fields from CMIP-class models or reanalysis data sets. This approach generates the large event sets needed for probabilistic risk analysis, including rare extreme events (Meiler et al., 2022; Baldwin et al., 2023; Fosu et al., 2024; Hemmati et al., 2025; Meiler et al., 2026), at lower cost than regional dynamical downscaling (Knutson et al., 2013; Patricola et al., 2017; Fu et al., 2019) or variable-resolution GCMs (Zarzycki et al., 2014; Stansfield et al., 2020).

We extend the CHAZ-based analysis of North Atlantic TC risk of Fosu et al. (2024), who downscaled 12 CMIP6 models (Eyring et al., 2016) under the SSP2-4.5, SSP3-7.0, and SSP5-8.5 scenarios, by adding the low-emissions SSP1-2.6 scenario. This extension enables comparison between the two extreme ends of the emissions spectrum (SSP1-2.6 and SSP5-8.5), and allows us to more fully explore the sensitivity of U.S. TC hazard risk to the level of warming. For reference, end-of-century (2080–2100) global mean temperature change relative to the 1995–2014 baseline is expected to be in the range of 1.23 ± 0.83°C for SSP1-2.6 and 3.99 ± 1.59°C for SSP5-8.5 (Riahi et al., 2017; Tebaldi et al., 2021). Our specific objectives are to: (1) project changes in North Atlantic TC genesis, tracks, and intensity; (2) quantify the evolving hazard of landfalling TCs to the U.S. coast; and (3) identify the factors that drive regional differences in projected North Atlantic TC risk. By linking projected North Atlantic TC activity to the spatial structure of environmental change in CMIP6 models, this study highlights the role of the pattern of warming, rather than just its magnitude, in shaping future regional TC activity and hazard.

The paper is structured as follows. Section 2 describes the CHAZ model, the CMIP6 data and bias correction, and the analysis methodology. In Section 3 we present our main findings as they relate to changes in North Atlantic landfall, followed by a discussion in Section 4 of how spatial patterns in the model's large-scale environmental fields shape the TC risks in both SSP scenarios.

2. Data and Methods

2.1. Downscaling CMIP6 Data with Columbia HAZard Model (CHAZ)

The Columbia HAZard model (CHAZ; (Lee et al., 2018)) is a statistical-dynamical downscaling model designed to link large-scale climate drivers to TC activity. Informed by background environmental forcing from climate model or observational reanalysis output, CHAZ consists of three distinct components that simulate storm genesis, track, and intensity.

The genesis component generates weak disturbances at a rate determined by environmental conditions, calculated using the Tropical Cyclone Genesis Index (TCGI) of Tippett, Camargo, and Sobel (2011) as modified by Camargo, Tippett, Sobel, Vecchi, and Zhao (2014). The seeding rate, μ_{MV}, is given by:

$$\mu_{MV} = \exp(b + b_{\eta}\eta_{850} + b_{MV}MV + b_{PI}PI + b_{Vshear}Vshear) \tag{1}$$

where the moisture variable (MV) is either column relative humidity (CRH) or saturation deficit (SD), following (Lee et al., 2020). Note that we only discuss results from TCGI calculated using CRH in the main text. The CRH version of CHAZ is the one that leads to increases in global TC frequency, and thus to greater hazard and risk. The two formulations differ substantially in the basin-wide magnitude of the projected change, but the along-coast pattern that is the subject of this study is common to both; we quantify this in Section 3.1 and report a comparison between CRH and SD projections in Figures S2 and S5. The coefficients b are constants, η_{850} is the 850 hPa absolute vorticity, PI is the potential intensity (Bister & Emanuel, 2002), and $Vshear$ is the deep layer vertical wind shear (850–250 hPa), calculated as the magnitude of difference in vector winds between the two pressure levels.

The coefficients for the TCGI used in this study have been updated from (Lee et al., 2018) and are derived from a Poisson regression using environmental fields from the fifth generation of the European Centre for Medium-Range Weather Forecasts (ECMWF) global atmospheric reanalysis (ERA5), (Hersbach et al., 2020) over the period 1981–2010, as described in Camargo et al. (2025). For TCGI-CRH, the coefficients are $b = -24.132$, $b_{\eta} = 2.512$, $b_{CRH} = 0.077$, $b_{PI} = 0.062$, and $b_{Vshear} = -0.120$. Further, following Camargo et al. (2025); Fosu et al. (2024), environmental predictors downscaled from CMIP6 (Eyring et al., 2016) used in the genesis component of the model, were bias-corrected by adjusting the monthly historical model climatology to match the ERA5 reanalysis climatology for the period 1981–2010, with the assumption of time-invariant biases applied to the CMIP6 future scenarios SSP1-2.6 and SSP5-8.5 (O'Neill et al., 2017) for years 2015 to 2100.

The track component of the model is based on a beta and advection model that moves storms via advection by a monthly mean environmental wind (defined as a weighted mean of a low-level [850 hPa] and an upper-tropospheric level [250 hPa]) along with a beta drift component (Emanuel et al., 2006), and a stochastic component based on eddy statistics to account for sub-monthly wind fluctuations. The intensity component is based on a multiple linear regression on key environmental parameters, with an auto-regressive stochastic error term to account for internal storm dynamics (Lee et al., 2015, 2016, 2018). A separate multiple linear regression model estimates intensity decay during and post-landfall (Lee et al., 2015, 2018). Since environmental predictors in the CHAZ's intensity module are normalized by the model's tropical mean, additional bias-correction as applied to TCGI predictors is not applied to the track and intensity predictor variables.

We downscaled CHAZ using output from 12 models that participated in CMIP6 (Eyring et al., 2016), as listed in Table S1. We utilized simulations from the historical scenario (HIST, 1951–2014; [from Fosu et al. (2024)]) and two future scenarios: the low-emissions scenario SSP1-2.6 (SSP126) and the high-emissions scenario SSP5-8.5 (SSP585) O'Neill et al. (2017)[TC tracks from Fosu et al. (2024)], both covering the period 2015–2100. While the downscaling was performed globally, this analysis focuses exclusively on TC activity in the North Atlantic basin (ATL, 0–55°N, 100–20°W).

For each CMIP6 model and scenario (HIST, SSP126, SSP585), we downscaled a single ensemble member as indicated in Table S1. For each of these runs, we applied 10 realizations of the random seeding process, each with 40 realizations of the stochastic intensity model, generating 400 unique synthetic TC event sets per model and scenario. This resulted in 25,600 synthetic years for the historical period (64 years × 400 combinations) and 34,400 synthetic years for the future period (86 years × 400 combinations) for each of the 12 models. For the North Atlantic basin, the historical period consists of a total of 122,474 storms, while the future period for SSP1-2.6 and SSP5-8.5 contains 192,048 and 189,390 storms respectively, a sample size necessary for robust probabilistic risk assessment (N. Lin & Emanuel, 2016). The synthetic track dataset includes storm position (longitude, latitude) and maximum sustained wind speed (kt) at six-hour intervals.

2.2. Estimating Changes to TC Landfall Hazard

To analyze landfall hazard, we defined seven landfall "gates" along the U.S. Atlantic and Gulf coastlines (Figure S1). The coastline data were obtained from the Natural Earth physical vector dataset (Kelso & Patterson, 2010). A landfall event was identified when a synthetic TC track intersected a coastline segment within a defined gate. To provide a compact representation of the typical tracks associated with landfalling storms in each coastal gate, we construct an average composite track from tracks across all models and track ensembles intersecting the defined coastal gate during the historical period (see Text S1, Figures 4c,d, tan solid).

Changes relative to the historical period from future projections (SSP1-2.6 and SSP5-8.5) are analyzed for three 20-year epochs: early-century (2030–2050), mid-century (2060–2080), and late-century (2080–2100). To evaluate the model's historical performance, we compared CHAZ downscaled data against the observed TC record from the International Best Track Archive for Climate Stewardship (IBTrACS version v04; (Knapp et al., 2010, 2018)).

To quantify the evolving TC hazard, we computed annual landfall frequencies and return periods (RPs) for different intensity thresholds at each gate based on the Saffir-Simpson wind scale. The annual frequency of exceedance for a given landfall wind speed threshold is the probability of one or more TCs making landfall with an intensity greater than that threshold in a given year. The RP (in years) for wind speeds exceeding this threshold is the inverse of this annual exceedance probability (AEP) for the corresponding gate.

We assess the change in hazard due to anthropogenic climate change using a "climate change delta" (cc-delta) approach from Fosu et al. (2024). The cc-delta for a specific TC statistic (e.g., landfall frequency of major hurricanes) is calculated as the difference between the future epoch mean and the historical period mean, normalized by the historical mean to express a percentage change:

$$\text{cc-delta} = \frac{\overline{X}_{\text{future}} - \overline{X}_{\text{historical}}}{\overline{X}_{\text{historical}}} \times 100\% \tag{2}$$

where $\overline{X}$ denotes the multi-model ensemble mean of the variable X. The mean values are calculated across the 12-model ensemble, with each model represented by the mean of its 400 realizations. To assess statistical significance, we applied a two-sided Student's t-test to the ensemble of model means (n=12) for historical and future periods, with a p-value of 0.05 serving as the significance threshold.

To separate the influence of storm genesis and track (steering), we use an empirical statistical method (e.g., Yokoi et al., 2013) to decompose the projected change in landfall frequency at a given coastal gate following Murakami, Wang, Li, and Kitoh (2013), by expressing the landfall frequency at a gate k as $F(k) = \int g(A_0)P(A_0,k)\,\mathrm{d}A_0$, where g is the TC genesis frequency in a source grid-cell A_0 and P the probability that a storm formed there, makes landfall at gate k. The projected future change in landfall frequency relative to the historical period at a given gate k can then be expressed as:

$$\delta F(k) = \int \Big[\underbrace{\delta g\, P_h}_{\text{genesis}} + \underbrace{g_h\, \delta P}_{\text{track}} + \underbrace{\delta g\, \delta P}_{\text{nonlinear}} \Big]_{A_0,\,k} \mathrm{d}A_0, \tag{3}$$

where the subscript h denotes the historical average, and δ, change between the future and historical reference period. The *genesis* term is the change that would have occurred had only the distribution of genesis changed, with the landfall probabilities held at their historical values; the *track* term is the converse; and the nonlinear term is the residual representing the combined effect of genesis and track changes to the gate landfall frequency $\delta F(k)$. The treatment in Equation 3 therefore identifies the "origins" of contributions to $\delta F(k)$ (Murakami et al., 2013), which is further discussed in Supplementary Information Text S2.

3. Results

3.1. Changes to Landfalling TC Risk

Figure 4 shows the multi-model mean change in North Atlantic tropical cyclone (TC) track density between the future and historical periods for SSP1-2.6 and SSP5-8.5. While basin-scale changes are spatially heterogeneous, a coherent and persistent regional signal emerges along the U.S. coastline. In particular, TC activity (including non-landfalling storms) decreases along much of the Gulf coastline, including the Texas region, while increasing along the Southeastern U.S. coast under both forcing scenarios. These patterns are evident throughout the 21st century and are amplified under the high-emission SSP5-8.5 scenario (Figure 4, Figure S2).

Regional changes in landfalling TC frequency are quantified in Figure 4 using the Texas and Southeast coastal gates. Across all three future periods, a reduction in TC frequency for the Texas gate is projected under both SSP1-2.6 and SSP5-8.5 (Figures 4a,b), with marginal increases in the near-term to significant decline across all storm categories especially in SSP5-8.5. The magnitude of the decrease grows with time and is consistently larger under SSP5-8.5. Ensemble-mean RP curves shift toward longer RP for frequent events, indicating a reduced likelihood of TC landfalls in the Texas region despite increasing inter-model spread (Figure S4a,b).

In contrast, the Southeast gate shows an increase in landfalling TC frequency under both scenarios (Figure 4 c,d). This increase is detectable as early as the near-term period (2030–2050) and strengthens toward the late 21st century (2080–2100), particularly under SSP5-8.5, with shortened Ensemble-mean RPs (Supplementary Information Figure S4 c,d). The opposing responses between the Texas and Southeast gates persist across scenarios, and is generally true of other gates in the U.S. Gulf region compared to those on the U.S. East coast (Supplementary Information, Figure S5).

These contrasting regional responses indicate that future TC risk along the U.S. coastline is neither spatially uniform, nor monotonically related to greenhouse gas forcing. Instead, changes in landfall frequency depend strongly on location, with the Gulf Coast and Southeast responding in opposite directions under both low- and high-emissions pathways.

We find the contrast between Gulf and East coast TC risk to be insensitive to the choice of moisture variable used in TCGI, although the basin-wide response using SD is substantially different compared to CRH (Lee et al., 2020; Fosu et al., 2024). The basin-wide TC frequency response is non-monotonic with increase in radiative forcing for CRH (Supplementary Information Text S3, Figures S2,S5). The late-century CRH response varies only weakly with forcing level, with the smallest increase occurring under SSP3-7.0, whereas the SD response decreases monotonically with increasing forcing (Figure S2b). One plausible explanation is the differing influence of greenhouse gas and aerosol forcing and its effect on TC activity (Ting et al., 2015; Sobel et al., 2016, 2019), since there are substantially greater aerosol emissions through the end of the century in SSP3-7.0 (Lund et al., 2019), than either SSP2-4.5 or SSP5-8.5 (Camargo et al., 2025).

Nevertheless, the contrast in regional TC risk is evident once the absolute difference in the basin-wide response is removed. For example, the difference in cc-deltas between the Southeast and Texas gates is positive (representing higher relative landfall risk in Southeast) for both formulations (CRH/SD) in every epoch and scenario, and grows with both time and forcing level, with all 12 (9) models agreeing in sign for SSP5-8.5 (SSP1-2.6) (Figure 4e–g). We therefore report CRH results throughout, while noting that conclusions drawn here concern the redistribution of landfall risk along the coast rather than the absolute basin-wide frequency change: the former is robust to the moisture formulation, the latter is not.

3.2. Basin-Scale Environmental Drivers of Regional TC Risk

To investigate the physical mechanisms underlying the contrasting regional landfall responses, Figures 4, 4 and 4 examine basin-wide TC track behavior together with changes in the large-scale environmental fields that determine that behavior in CHAZ. Figure 4c,d shows the average TC track density for storms making landfall in the Texas and Southeast gates. Texas-landfalling storms are concentrated over the western Atlantic, Gulf of Mexico and Caribbean, whereas Southeast-landfalling storms are distributed across the central and eastern Main Development Region (MDR) defined between 10°–20°N latitude, and 20°–85°W longitude. Track density is, however, a result of storm genesis and track combined, and cannot by itself be used to make an attribution of the change in landfall frequency to either process. We therefore apply the decomposition of Equation 3 to separate the two.

Figure 4 shows the decomposition of projected change in landfall frequency for the late-century period. At the Southeast gate the projected increase is almost entirely a genesis effect: the genesis term contributes

+18.6% under SSP1-2.6 and +12.8% under SSP5-8.5, against track contributions of only −1.0% and −1.6%. The origin maps locate these positive contributions (primarily as genesis change) in the subtropical western Atlantic and the central-to-eastern MDR (Figure 4g,j), also evidenced by track density (Figure 4c,d). Under SSP1-2.6 the Texas genesis term is positive (+6.0%) but is offset by a negative track term (−7.6%), leaving the net change small (−1.4%), substantiated by near-zero cc-deltas (Figure 4a). However, in SSP5-8.5 genesis and track account for −14.9% and −13.6% respectively, spatially almost entirely within the Gulf of Mexico and Western MDR (Figure 4d,e). Fewer storms therefore form in the Gulf and Caribbean under the warmer scenario, and a smaller fraction of those that do form reach the Texas coast, whereas storms landfalling in the Southeast increasingly originate in the MDR and subtropical Atlantic. Contributions from both terms are positive or near-neutral in the early-century epoch, and turn strongly negative thereafter (Supporting Information, Figure S7), accounting for the transition from a near-term increase to a late-century decline in landfall frequency (Figure 4b). The nonlinear term does not exceed 5.1% of the historical frequency at either gate, making the combined effect of future genesis and track change at the storm origin minimal.

Next, we consider basin-wide changes late-century changes in potential intensity (PI) normalized by global mean temperature change, vertical wind shear (850–250 hPa), and steering flow for SSP1-2.6 and SSP5-8.5. This PI pattern change in the tropical Atlantic characterized by a broadly positive basin-wide increase is very robust and present in multiple versions of CMIP (e.g., Vecchi & Soden, 2007a; Camargo, 2013; Ting et al., 2015; Sobel et al., 2016; Camargo et al., 2025).

Across both scenarios, vertical wind shear increases over the western Atlantic, Gulf of Mexico, and Caribbean (western MDR), while weakening across portions of the central and eastern MDR (Figure 4 c,d). This pattern is known to be present across future scenarios in past and current CMIP versions (e.g. Vecchi and Soden (2007a); Camargo (2013); Sobel et al. (2016); Ting, Kossin, Camargo, and Li (2019); Camargo et al. (2025)). The representative tracks for Texas-landfalling storms intersect regions of enhanced shear, whereas Southeast-landfalling tracks pass through regions of reduced shear. This spatial contrast is more pronounced under SSP5-8.5, consistent with the larger magnitude changes in landfall frequency seen in Figure 4. Storms whose pathways cross the central MDR region and western North Atlantic basin, which show future reduction in deep-layer (850–250 hPa) vertical wind shear, with conducive conditions for intensification, lead to increased potential landfall risk in the Southeast (Figures 4 c,d, and 4g-i). Changes in PI exhibit a broadly positive signal across much of the tropical Atlantic, indicating an overall thermodynamic environment more favorable for TC intensification. PI increases are broadly distributed across the basin, with comparatively modest spatial structure, including a local minimum in the MDR in both SSPs (Figure 4a,b). While enhanced PI may support increased TC hazard in both the coastal regions of the Southeast and Texas, the shear signal is more directly consistent with the contrasting responses in landfall risk between the two regions (Figure 4 a,b versus c,d), supported by the origin decomposition contributions at both gates (Figure 4).

TC motion is largely governed by the surrounding deep-layer synoptic-scale flow structure (Chan & Gray, 1982; Holland, 1983; Chan, 2005). Regardless of the emission scenario considered here, we find that shifts in large-scale atmospheric steering winds alter storm tracks and forward speeds, ultimately leading to changes in the landfall risk for different coastal regions. The projected changes in steering flow (Figure 4e,f) exhibit a coherent basin-scale pattern characterized by enhanced easterly flow across the tropical Atlantic and Caribbean. While the magnitude of the anomalies is more pronounced under SSP5-8.5, the overall structure in the vector winds is consistent between SSP1-2.6 and SSP5-8.5. The resulting steering anomalies in both direction and magnitude tend to favor storm propagation across the central MDR towards the western North Atlantic basin and the Southeast U.S. coastline, while reducing the likelihood that westward tracking storms find favorable steering patterns within the western Caribbean and Gulf of Mexico. In combination with the spatial distribution of vertical wind shear and PI anomalies, these circulation changes reinforce the divergence in regional TC risk between the two coastlines by influencing the movement and tracking of storms in the basin (Figures 4 track term, 4c,d).

The shear patterns resemble an El Niño–like response in the large-scale climate system, characterized by increased vertical wind shear over the western Atlantic and reduced shear across the central MDR (Gray, 1984; Goldenberg & Shapiro, 1996; Aiyyer & Thorncroft, 2006; Vecchi & Soden, 2007b; Tippett et al., 2025). Such a pattern is known to suppress Atlantic TC activity in regions influenced by stronger shear while favoring genesis and intensification where shear is reduced (Gray, 1984; Patricola et al., 2014; Tang & Neelin, 2004; Klotzbach, 2011; Rios-Berrios et al., 2024). In this framework, the El Niño–like forced response preferentially enhances TC activity along Southeast-oriented pathways while suppressing activity for storms tracking toward the Gulf Coast.

Together, these results indicate that forced changes in basin-scale environmental fields—particularly vertical wind shear—play a central role in shaping the regional redistribution of landfalling TC risk. The persistence of these patterns across SSP1-2.6 and SSP5-8.5 (Figures 4, 4) suggests that regional TC risk along the U.S. is more sensitive to large-scale circulation changes and pattern of surface warming, than to the degree of global warming per se.

4. Discussion and Conclusions

This study identifies a robust, forced redistribution of North Atlantic tropical cyclone landfall risk along the U.S. coastline under both low- and high-emissions scenarios. Using simulations with a statistical-dynamical downscaling model driven by 12 Earth system models from CMIP6 (Table S1), we find a consistent decrease in landfalling TC frequency in the Gulf of Mexico, particularly the Texas coastline, alongside an increase along the Southeastern U.S. coast (Figures 4 a-d and 4). These opposing regional responses persist across SSP1-2.6 and SSP5-8.5, differing primarily in magnitude rather than sign. This indicates that mitigation pathway alone does not determine the spatial pattern of future TC risk, underscoring the importance of regional-scale assessment for adaptation planning.

The contrasting landfall responses appear closely linked to basin-wide changes in large-scale environmental conditions that influence TC genesis, intensification, and steering. In particular, changes in vertical wind shear emerge as a dominant factor shaping regional outcomes. Storms that ultimately make landfall along the Southeast preferentially traverse regions where vertical wind shear weakens in the future climate, enhancing TC favorability (Figures 4g-i and 4c,d). In contrast, Texas- and Gulf Coast–bound storms encounter regions of higher shear, which suppresses the formation of storms within the Gulf and Western MDR, with a smaller fraction of them making landfall, both contributing to the projected landfall frequency decrease in the Texas-Gulf region (Figure 4d,e,n). While potential intensity generally increases across much of the tropical Atlantic, its spatial gradients are comparatively weak and do not offset the strongly regional nature of the shear response. While these basin-scale patterns of change in PI and vertical wind shear are consistent with results from previous CMIP3 (Vecchi & Soden, 2007a, 2007b) and CMIP5 models (Camargo, 2013; Ting et al., 2015, 2019; Sobel et al., 2016), as well as CMIP6 models (Camargo et al., 2025), here we demonstrate their linkage to regional differences in landfalling TC activity for the North Atlantic basin.

The spatial structure of the projected environmental changes over the Atlantic, particularly the increase in vertical shear over the western Atlantic, resembles those associated with El Niño events. This suggests that these shear changes are associated with the broadly El Niño-like pattern of change in the tropical Pacific SST trends in the models, characterized by weakened zonal SST gradients. On interannual timescales, the vertical shear anomalies play an important role in modulating North Atlantic TC activity (Gray, 1984; Goldenberg & Shapiro, 1996; Klotzbach, 2011; Patricola et al., 2014; Smith et al., 2007; Pielke & Landsea, 1999; Kossin et al., 2010). Our results suggest that analogous circulation changes arise as part of the forced climate response, effectively imprinting an El Niño-like trend onto the pattern of Atlantic TC activity. This pattern strengthens with warming, such that TC hazard along the Gulf coast is more suppressed in SSP5-8.5 than in SSP1-2.6, even as TC hazard increases more in SSP5-8.5 than in SSP1-2.6 along the Atlantic coast of the southeast US. Southeast-favoring storm tracks increasingly align with regions of reduced shear, while Gulf-oriented tracks encounter increased shear, producing the divergent landfall trends identified in this study.

Several limitations warrant consideration. Our analysis focuses on landfalling TC frequency rather than intensity, rainfall, or compound hazards, which may respond differently to environmental forcing. While the CHAZ framework captures key large-scale controls on TC activity, the robustness of the El-Niño–like mean-state response in CMIP6 projections remains an active area of inquiry. Recent work highlights observed trends over the historical period that are more similar in pattern to La Niña than to El Niño, with cooling in the eastern Equatorial Pacific and strengthened zonal gradients, in strong contrast to simulations (Seager et al., 2019, 2022; Wills et al., 2022; Zhuo et al., 2025). Models also disagree in projected ENSO characteristics with no clear consensus on future changes in ENSO frequency, amplitude structure (e.g., C. Wang et al., 2017; Cai et al., 2021; Erickson & Patricola, 2023; Zhuo et al., 2025). Consequently, while the ENSO-like circulation pattern provides a useful dynamical framework for interpreting the environmental changes identified here, the degree to which the pattern of TC hazard identified in the simulations here will emerge in the real climate system remains highly uncertain. On the other hand, the broader conclusion is that the pattern of SST change is more important than the global mean warming to regional TC hazard and risk. This might well remain true even if the sign of the pattern change were reversed, and thus is, in our view, more likely to be a robust conclusion. Furthermore, the inferred *cc-delta* signal depends on the baseline distribution of TC genesis and track pathways in the model. If the models exhibit specific regional biases which differ from the observed TC regional climatology, the resulting deltas could be biased too. While a bias-correction is applied to match the observed frequency of landfalling storms within each coastal gate, residual biases in the spatial distribution of genesis and track pathways may still influence the magnitude of the projected changes.

These findings also highlight that future TC risk cannot be inferred solely from basin-wide metrics such as total TC frequency or mean intensity. Changes in large-scale circulation patterns can reorganize where storms preferentially form, intensify, and move, leading to persistent regional contrasts in landfall risk even when the overall basin response is muted or uncertain (Knutson et al., 2020; Sobel et al., 2021; Camargo et al., 2023). The origin decomposition (Equation 3) makes this explicit: the net change at a given gate is the residual of larger and partially offsetting genesis and track contributions (Figure 4m,n), so a small net change at a coastline does not imply a correspondingly small forced response. The persistence of the Gulf-Atlantic TC hazard contrast across emissions scenarios suggests that internal variability and regional circulation responses may exert a stronger control on future landfall risk than the magnitude of warming or emissions pathways alone. Future work should examine how internal climate variability, including from combined effects of ENSO and Atlantic Multi-decadal Oscillation and their modulation under warming, may interact with the forced response identified here to influence decadal-scale fluctuations in regional TC risk.

In summary, our results demonstrate that regional TC landfall risk along the U.S. coastline is highly sensitive to large-scale SST pattern and circulation changes under climate change. The opposing responses between the Gulf Coast and Southeast persist even under strong mitigation, emphasizing that adaptation strategies must account for geographically specific risk trajectories rather than relying on basin-wide projections alone.

Open Research Statement

The IBTrACS dataset can be downloaded from `www.ncei.noaa.gov/products/international-best-track-archive`. The publicly available CMIP6 multi-model ensemble dataset was used in this paper. CMIP6 ensemble model outputs can be downloaded from the different Earth System Grid Federation (ESGF) nodes. CHAZ is an open-source model and can be downloaded from `github.com/cl3225/CHAZ`.

Acknowledgements:
RL, AHS, SJC, CYL and MKT acknowledge funding support for this work by Aon plc.

References

Aiyyer, A., & Thorncroft, C. (2006). Climatology of vertical wind shear over the tropical Atlantic. *Journal of Climate*, *19*(12), 2969–2983. doi: 10.1175/JCLI3685.1

Baldwin, J. W., Lee, C.-Y., Walsh, B. J., Camargo, S. J., & Sobel, A. H. (2023). Vulnerability in a tropical cyclone risk model: Philippines case study. *Weather, Climate, and Society*, *15*, 503–523. doi: 10.1175/WCAS-D-22-0049.1

Bengtsson, L., Botzet, M., & Esch, M. (1996). Will greenhouse gas-induced warming over the next 50 years lead to higher frequency and greater intensity of hurricanes? *Tellus A*, *48*(1), 57-73. doi: https://doi.org/10.1034/j.1600-0870.1996.00004.x

Bister, M., & Emanuel, K. A. (2002). Low frequency variability of tropical cyclone potential intensity 1. interannual to interdecadal variability. *Journal of Geophysical Research: Atmospheres*, *107*(D22), 4621. doi: 10.1029/2001JD000780

Bloemendaal, N., Haigh, I. D., de Moel, H., Muis, S., Haarsma, R. J., & Aerts, J. C. J. H. (2020). Generation of a global synthetic tropical cyclone hazard dataset using STORM. *Scientific Data*, *7*, 40. doi: 10.1038/s41597-020-0381-2

Broccoli, A. J., & Manabe, S. (1990). Can existing climate models be used to study anthropogenic changes in tropical cyclone climate? *Geophysical Research Letters*, *17*(11), 1917-1920. doi: https://doi.org/10.1029/GL017i011p01917

Cai, W., Santoso, A., Collins, M., Dewitte, B., Karamperidou, C., Kug, J.-S., … Zhong, W. (2021, September). Changing El Niño–Southern Oscillation in a warming climate. *Nature Reviews Earth and Environment*, *2*(9), 628–644. (Published online: 17 August 2021) doi: 10.1038/s43017-021-00199-z

Camargo, S. J. (2013). Global and regional aspects of tropical cyclone activity in the CMIP5 models. *Journal of Climate*, *26*, 9880–9902. doi: 10.1175/JCLI-D-12-00549.1

Camargo, S. J., et al. (2023). An update on the influence of natural climate variability and anthropogenic climate change on tropical cyclones. *Tropical Cyclone Research and Review*, *12*, 216–239. doi: 10.1016/j.tcrr.2023.10.001

Camargo, S. J., Robertson, A. W., Gaffney, S. J., Smyth, P., & Ghil, M. (2007, July 15). Cluster analysis of typhoon tracks. Part I: General properties. *Journal of Climate*, *20*(14), 3635–3653. (Print publication: 15 July 2007) doi: 10.1175/JCLI4188.1

Camargo, S. J., Sobel, A. H., Barnston, A. G., & Emanuel, K. A. (2007). Tropical cyclone genesis potential index in climate models. *Tellus A*, *59*, 428–443. doi: 10.1111/j.1600-0870.2007.00238.x

Camargo, S. J., Ting, M., & Kushnir, Y. (2013). Influence of local and remote SST on North Atlantic tropical cyclone potential intensity. *Climate Dynamics*, *40*(5-6), 1515–1529. doi: 10.1007/s00382-012-1536-4

Camargo, S. J., Tippett, M. K., Sobel, A. H., Lee, C.-Y., Fosu, B., & Hodges, K. I. (2025). Tropical cyclones and associated environmental fields in CMIP6 models. *Journal of Climate*, *38*, 3877–3902. doi: 10.1175/JCLI-D-24-0629.1

Camargo, S. J., Tippett, M. K., Sobel, A. H., Vecchi, G. A., & Zhao, M. (2014). Testing the performance of tropical cyclone genesis indices in future climates using the HiRAM model. *Journal of Climate*, *27*, 9171–9196. doi: 10.1175/JCLI-D-13-00505.1

Chan, J. C. L. (2005). The physics of tropical cyclone motion. *Annual Review of Fluid Mechanics*, *37*, 99–128. doi: 10.1146/annurev.fluid.37.061903.175702

Chan, J. C. L., & Gray, W. M. (1982, October 1). Tropical cyclone movement and surrounding flow relationships. *Monthly Weather Review*, *110*(10), 1354–1374. (Print publication: 1 October 1982) doi: 10.1175/1520-0493(1982)110<1354:TCMASF>2.0.CO;2

Chavas, D. R., Camargo, S. J., & Tippett, M. K. (2025). Tropical cyclone genesis potential using a ventilated potential intensity. *Journal of Climate*, *38*, 1667–1689. doi: 10.1175/JCLI-D-24-0186.1

Colbert, A. J., Soden, B. J., Vecchi, G. A., & Kirtman, B. P. (2013). The impact of anthropogenic climate change on North Atlantic tropical cyclone tracks. *Journal of Climate*, *26*(12), 4088–4104.

Daloz, A. S., et al. (2015). Cluster analysis of downscaled and explicitly simulated North Atlantic tropical cyclone tracks. *Journal of Climate*, *28*(4), 1333–1361. doi: 10.1175/JCLI-D-13-00646.1

Emanuel. (1987). The dependence of hurricane intensity on climate. *Nature*, *326*, 483–485. doi: 10.1038/326483a0

Emanuel, Ravela, S., Vivant, E., & Risi, C. (2006). A statistical deterministic approach to hurricane risk assessment. *Bulletin of the American Meteorological Society*, *87*(3), 299–314. Retrieved from https://doi.org/10.1175/BAMS-87-3-299 doi: 10.1175/BAMS-87-3-299

Emanuel, K. A. (2013). Downscaling CMIP5 climate models shows increased tropical cyclone activity over the 21st century. *Proceedings of the National Academy of Sciences*, *110*, 12219–12224. doi: 10.1073/pnas.1301293110

Emanuel, K. A., Sundararajan, R., & Williams, J. (2008). Hurricanes and global warming: Results from downscaling IPCC AR4 simulations. *Bulletin of the American Meteorological Society*, *89*, 347–367. doi: 10.1175/BAMS-89-3-347

Erickson, N. E., & Patricola, C. M. (2023, February 16). Future projections of the El Niño–Southern Oscillation and Tropical Pacific mean state in CMIP6. *Journal of Geophysical Research: Atmospheres*, *128*(3), e2022JD037563. (Article e2022JD037563) doi: 10.1029/2022JD037563

Eyring, V., Bony, S., Meehl, G. A., Senior, C. A., Stevens, B., Stouffer, R. J., & Taylor, K. E. (2016). Overview of the coupled model intercomparison project phase 6 (CMIP6) experimental design and organization. *Geoscientific Model Development*, *9*, 1937–1958. doi: 10.5194/gmd-9-1937-2016

Fosu, B. O., et al. (2024). Assessing future tropical cyclone risk using downscaled CMIP6 projections. *Journal of Catastrophe Risk and Resilience*, *2024*(2), 1. doi: 10.63024/dpva-2pa1

Fu, D., Chang, P., Patricola, C. M., & Saravanan, R. (2019). High-resolution tropical channel model simulations of tropical cyclone climatology and intraseasonal-to-interannual variability. *Journal of Climate*, *32*, 7871–7895. doi: 10.1175/JCLI-D-19-0130.1

Goldenberg, S. B., & Shapiro, L. J. (1996). Physical mechanisms for the association of El Niño and west African rainfall with Atlantic major hurricane activity. *Journal of Climate*, *9*(6), 1169–1187. Retrieved from https://doi.org/10.1175/1520-0442(1996)009<1169:PMFTAO>2.0.CO;2 doi: 10.1175/1520-0442(1996)009<1169:PMFTAO>2.0.CO;2

Gray, W. M. (1968, October 1). Global view of the origin of tropical disturbances and storms. *Monthly Weather Review*, *96*(10), 669–700. (Print publication: 1 October 1968) doi: 10.1175/1520-0493(1968)096<0669:GVOTOO>2.0.CO;2

Gray, W. M. (1984). Atlantic seasonal hurricane frequency. Part I: El Niño and 30 mb quasi-biennial oscillation influences. *Monthly Weather Review*, *112*(9), 1649–1668. doi: 10.1175/1520-0493(1984)112<1649:ASHFPI>2.0.CO;2

Hemmati, M., Lee, C.-Y., Mandli, K. T., Sobel, A. H., Camargo, S. J., & Sustiel, J. (2025, October 6). Assessment of Caribbean coastal hazard posed by tropical cyclones. *Journal of Applied Meteorology and Climatology*, *64*(11), 1681–1694. doi: 10.1175/JAMC-D-24-0138.1

Hersbach, H., et al. (2020). The ERA5 global reanalysis. *Quarterly Journal of the Royal Meteorological Society*, *146*, 1999–2049. doi: 10.1002/qj.3803

Holland, G. J. (1983). Tropical cyclone motion: Environmental interaction plus a beta effect. *Journal of the Atmospheric Sciences*, *40*(2), 328–342. doi: 10.1175/1520-0469(1983)040<0328:TCMEIP>2.0.CO;2

Jewson, S. (2024). Projecting future tropical cyclone frequencies by combining uncertain empirical estimates of baseline frequencies with climate model estimates of change. *Journal of Catastrophe Risk and Resilience*, *02*(3). doi: 10.63024/m9wk-3420

Jing, R., & Lin, N. (2020). An environment-dependent probabilistic tropical cyclone model. *Journal of Advances in Modeling Earth Systems*, *12*(4), e2019MS001975. doi: 10.1029/2019MS001975

Jones, C. G., & Thorncroft, C. D. (1998). The role of el niño in Atlantic tropical cyclone activity. *Weather*, *53*(9), 324-336. Retrieved from https://rmets.onlinelibrary.wiley.com/doi/abs/10.1002/j.1477-8696.1998.tb06409.x doi: https://doi.org/10.1002/j.1477-8696.1998.tb06409.x

Kelso, N. V., & Patterson, T. (2010). Introducing natural earth data-naturalearthdata.com. *Geographia Technica*, *5*, 82–89.

Klotzbach, P. J. (2011). The influence of El Niño–Southern Oscillation and the Atlantic Multidecadal Oscillation on Caribbean tropical cyclone activity. *Journal of Climate*, *24*(3), 721–731. Retrieved from https://doi.org/10.1175/2010JCLI3705.1 doi: 10.1175/2010JCLI3705.1

Knapp, K. R., Diamond, H. J., Kossin, J. P., Kruk, M. C., & Schreck, C. J. I. (2018). International best track archive for climate stewardship (IBTrACS) project, version 4.

(Accessed 16 July 2024) doi: 10.25921/82TY-9E16

Knapp, K. R., Kruk, M. C., Levinson, D. H., Diamond, H. J., & Neumann, C. J. (2010). The international best track archive for climate stewardship (IBTrACS): Unifying tropical cyclone data. *Bulletin of the American Meteorological Society*, *91*, 363–376. doi: 10.1175/2009BAMS2755.1

Knutson, T. R., Camargo, S. J., Chan, J. C. L., Emanuel, K., Ho, C.-H., Kossin, J., … Wu, L. (2020). Tropical cyclones and climate change assessment: Part II: Projected response to anthropogenic warming. *Bulletin of the American Meteorological Society*, *101*, E303–E322. doi: 10.1175/BAMS-D-18-0194.1

Knutson, T. R., McBride, J., & Chan, J. (2010). Tropical cyclones and climate change. *Nature Geoscience*, *3*, 157–163. doi: 10.1038/ngeo779

Knutson, T. R., Sirutis, J. J., Vecchi, G. A., Garner, S., Zhao, M., Kim, H.-S., ... Villarini, G. (2013). Dynamical downscaling projections of twenty-first-century atlantic hurricane activity: CMIP3 and CMIP5 model-based scenarios. *Journal of Climate*, *26*(17), 6591–6617. doi: 10.1175/JCLI-D-12-00539.1

Knutson, T. R., Sirutis, J. J., Zhao, M., Tuleya, R. E., Bender, M., Vecchi, G. A., ... Chavas, D. (2015, September 11). Global projections of intense tropical cyclone activity for the late twenty-first century from dynamical downscaling of CMIP5/RCP4.5 scenarios. *Journal of Climate*, *28*(18), 7203–7224. (Published online: 11 September 2015) doi: 10.1175/JCLI-D-15-0129.1

Kossin, J. P., Camargo, S. J., & Sitkowski, M. (2010). Climate modulation of North Atlantic hurricane tracks. *Journal of Climate*, *23*, 3057–3076. doi: 10.1175/2010JCLI3497.1

Landsea, C. W., Pielke, R. A., Mestas-Nuñez, A. M., & Knaff, J. A. (1999, May). Atlantic basin hurricanes: Indices of climatic changes. *Climatic Change*, *42*(1), 89–129. (Published: 25 May 1999) doi: 10.1023/A:1005416332322

Lee, Camargo, S. J., Sobel, A. H., & Tippett, M. K. (2020). Statistical–dynamical downscaling projections of tropical cyclone activity in a warming climate: Two diverging genesis scenarios. *Journal of Climate*, *33*, 4815–4834. doi: 10.1175/JCLI-D-19-0452.1

Lee, Tippett, M. K., Camargo, S. J., & Sobel, A. H. (2015). Probabilistic multiple linear regression modeling for tropical cyclone intensity. *Monthly Weather Review*, *143*, 933–954. doi: 10.1175/MWR-D-14-00171.1

Lee, Tippett, M. K., Sobel, A. H., & Camargo, S. J. (2016). Autoregressive modeling for tropical cyclone intensity climatology. *Journal of Climate*, *29*, 7815–7830. doi: 10.1175/JCLI-D-15-0909.1

Lee, Tippett, M. K., Sobel, A. H., & Camargo, S. J. (2018). An environmentally forced tropical cyclone hazard model. *Journal of Advances in Modeling Earth Systems*, *10*, 223–241. doi: 10.1002/2017MS001186

Lin, J., Lee, C.-Y., Camargo, S. J., et al. (2025). The response of tropical cyclone hazard to natural and forced patterns of warming. *npj Climate and Atmospheric Science*, *8*, 109. (Article number 109) doi: 10.1038/s41612-025-00997-y

Lin, N., & Emanuel, K. (2016, January). Grey swan tropical cyclones. *Nature Climate Change*, *6*, 106–111. Retrieved from https://doi.org/10.1038/nclimate2777 doi: 10.1038/nclimate2777

Lund, M. T., Myhre, G., & Samset, B. H. (2019). Anthropogenic aerosol forcing under the shared socioeconomic pathways. *Atmospheric Chemistry and Physics*, *19*, 13827–13839. doi: 10.5194/acp-19-13827-2019

Meiler, S., Lee, C.-Y., Camargo, S. J., et al. (2026). Global coastal wind hazard maps from the CHAZ tropical cyclone model. *Scientific Data*, *13*(1), 136. (Article number 136) doi: 10.1038/s41597-025-06452-0

Meiler, S., Vogt, T., Bloemendaal, N., Ciullo, A., Lee, C.-Y., Camargo, S. J., ... Bresch, D. N. (2022). Intercomparison of regional loss estimates from global synthetic tropical cyclone models. *Nature Communications*, *13*, 6156. doi: 10.1038/s41467-022-33918-1

Murakami, H., & Wang, B. (2010). Future change of North Atlantic tropical cyclone tracks: Projection by a 20-km-mesh global atmospheric model. *Journal of Climate*, *23*(10), 2699–2721. doi: 10.1175/2010JCLI3338.1

Murakami, H., Wang, B., Li, T., & Kitoh, A. (2013). Projected increase in tropical cyclones near Hawaii. *Nature Climate Change*, *3*(8). doi: 10.1038/nclimate1890

Nakamura, J., Camargo, S. J., Sobel, A. H., Emanuel, K. A., Kumar, A., LaRow, T. E., et al. (2017). Western North Pacific tropical cyclone model tracks in present and future climates. *Journal of Geophysical Research: Atmospheres*, *122*, 9721–9744. doi: 10.1002/2017JD027007

O'Neill, B. C., Kriegler, E., Ebi, K. L., Kemp-Benedict, E., Riahi, K., Rothman, D. S., ... Solecki, W. (2017). The roads ahead: Narratives for shared socioeconomic pathways describing world futures in the 21st century. *Global Environmental Change*, *42*, 169-180. Retrieved from https://www.sciencedirect.com/science/article/pii/S0959378015000060 doi: https://doi.org/10.1016/j.gloenvcha.2015.01.004

Patricola, C. M., Saravanan, R., & Chang, P. (2014). The impact of the El Niño–Southern Oscillation and Atlantic Meridional Mode on seasonal atlantic tropical cyclone activity. *Journal of Climate*, *27*, 5311–5328. doi: 10.1175/JCLI-D-13-00687.1

Patricola, C. M., Saravanan, R., & Chang, P. (2017). A teleconnection between atlantic sea surface temperature and eastern and central North Pacific tropical cyclones. *Geophysical Research Letters*, *44*, 1167–1174. doi: 10.1002/2016GL071965

Pielke, R. A., & Landsea, C. N. (1999). La Niña, El Niño, and Atlantic Hurricane Damages in the United States. *Bulletin of the American Meteorological Society*, *80*(10), 2027–2034. Retrieved from https://doi.org/10.1175/1520-0477(1999)080<2027:LNAENO>2.0.CO;2 (Corrected journal title from "Bulletin America Meteorology Social") doi: 10.1175/1520-0477(1999)080<2027:LNAENO>2.0.CO;2

Ramsay, H. A., & Sobel, A. H. (2011). Effects of relative and absolute sea surface temperature on tropical cyclone potential intensity using a single-column model. *Journal of Climate*, *24*(1), 183–193. doi: 10.1175/2010JCLI3691.1

Riahi, K., van Vuuren, D. P., Kriegler, E., Edmonds, J., O'Neill, B. C., Fujimori, S., ... Tavoni, M. (2017). The shared socioeconomic pathways and their energy, land use, and greenhouse gas emissions implications: An overview. *Global Environmental Change*, *42*, 153-168. Retrieved from https://www.sciencedirect.com/science/article/pii/S0959378016300681 doi: https://doi.org/10.1016/j.gloenvcha.2016.05.009

Rios-Berrios, R., Finocchio, P. M., Alland, J. J., Chen, X., Fischer, M. S., Stevenson, S. N., & Tao, D. (2024). A review of the interactions between tropical cyclones and environmental vertical wind shear. *Journal of the Atmospheric Sciences*, *81*(4), 713–741. doi: 10.1175/JAS-D-23-0022.1

Saunders, M. A., Chandler, R. E., Merchant, C. J., & Roberts, F. P. (2000). Atlantic hurricanes and NW pacific typhoons: ENSO spatial impacts on occurrence and landfall. *Geophysical Research Letters*, *27*(8), 1147–1150. doi: 10.1029/1999GL010948

Seager, R., Cane, M., Henderson, N., Lee, D.-E., Abernathey, R., & Zhang, H. (2019). Strengthening Tropical Pacific zonal sea surface temperature gradient consistent with rising greenhouse gases. *Nature Climate Change*, *9*, 517–522. doi: 10.1038/s41558-019-0505-x

Seager, R., Henderson, N., & Cane, M. (2022). Persistent discrepancies between observed and modeled trends in the Tropical Pacific ocean. *Journal of Climate*, *35*, 4571–4584. doi: 10.1175/JCLI-D-21-0648.1

Smith, S. R., Brolley, J., O'Brien, J. J., & Tartaglione, C. A. (2007). ENSO's impact on regional U.S. hurricane activity. *Journal of Climate*, *20*(7), 1404–1414. doi: 10.1175/JCLI4063.1

Sobel, A. H., Camargo, S. J., Hall, T. M., Lee, C.-Y., Tippett, M. K., & Wing, A. A. (2016). Human influence on tropical cyclone intensity. *Science*, *353*, 242–246. doi: 10.1126/science.aaf6574

Sobel, A. H., Lee, C.-Y., Camargo, S. J., Mandli, K. T., Emanuel, K. A., Mukhopadhyay, P., & Mahakur, M. (2019). Tropical cyclone hazard to Mumbai in the recent historical climate. *Monthly Weather Review*, *147*, 2355–2366. doi: 10.1175/MWR-D-18-0419.1

Sobel, A. H., et al. (2023). Near-term tropical cyclone risk and coupled earth system model biases. *Proceedings of the National Academy of Sciences*, *120*(4), e2209631120. doi: 10.1073/pnas.2209631120

Sobel, A. H., Wing, A. A., Camargo, S. J., Patricola, C. M., Vecchi, G. A., Lee, C.-Y., & Tippett, M. K. (2021). Tropical cyclone frequency. *Earth's Future*, *9*(12), e2021EF002275. doi: 10.1029/2021EF002275

Stansfield, A. M., Reed, K. A., & Zarzycki, C. M. (2020). Changes in precipitation from North Atlantic tropical cyclones under RCP scenarios in the variable-resolution Community Atmosphere Model. *Geophysical Research Letters*, *47*(4), e2019GL086930. doi: 10.1029/2019GL086930

Tang, B. H., & Neelin, J. D. (2004). ENSO influence on atlantic hurricanes via tropospheric warming. *Geophysical Research Letters*, *31*(24), L24204. doi: 10.1029/2004GL021072

Tebaldi, C., et al. (2021). Climate model projections from the scenario model intercomparison project (ScenarioMIP) of CMIP6. *Earth System Dynamics*, *12*, 253–293. doi: 10.5194/esd-12-253-2021

Ting, M., Camargo, S. J., Li, C., & Kushnir, Y. (2015, May 15). Natural and forced North Atlantic hurricane potential intensity change in CMIP5 models. *Journal of Climate*, *28*(10), 3926–3942. doi: 10.1175/JCLI-D-14-00520.1

Ting, M., Kossin, J. P., Camargo, S. J., & Li, C. (2019). Past and future hurricane intensity change along the U.S. East Coast. *Scientific Reports*, *9*, 7795. doi: 10.1038/s41598-019-44252-w

Tippett, M. K., Becker, E. J., Camargo, S. J., García-Franco, J. L., Lee, C.-Y., & L'Heureux, M. L. (2025). Relation of atlantic tropical cyclone activity with observed and predicted ENSO indices. *Geophysical Research Letters*, *52*(9), e2025GL119286. (Article e2025GL119286) doi: 10.1029/2025GL119286

Tippett, M. K., Camargo, S. J., & Sobel, A. H. (2011). A poisson regression index for tropical cyclone genesis and the role of large-scale vorticity in genesis. *Journal of Climate*, *24*, 2335–2357. doi: 10.1175/2010JCLI3811.1

Vecchi, G. A., Delworth, T. L., Murakami, H., Underwood, S. D., Wittenberg, A. T., Zeng, F., … Yang, X. (2019, November). Tropical cyclone sensitivities to CO2 doubling: Roles of atmospheric resolution, synoptic variability and background climate changes. *Climate Dynamics*, *53*(9), 5999–6033. (Published: 12 August 2019) doi: 10.1007/s00382-019-04913-y

Vecchi, G. A., & Soden, B. J. (2007a). Effect of remote sea surface temperature change on tropical cyclone potential intensity. *Nature*, *450*, 1066–1070. doi: 10.1038/nature06423

Vecchi, G. A., & Soden, B. J. (2007b). Increased Tropical Atlantic wind shear in model projections of global warming. *Geophysical Research Letters*, *34*(8), L08702. doi: 10.1029/2006GL028905

Walsh, K. J. E., et al. (2016). Tropical cyclones and climate change. *Wiley Interdisciplinary Reviews: Climate Change*, *7*, 65–89. doi: 10.1002/wcc.371

Wang, B., & Chan, J. C. L. (2002). How strong ENSO events affect tropical storm activity over the Western North Pacific. *Journal of Climate*, *15*, 1643–1658. doi: 10.1175/1520-0442(2002)015<1643:HSEEAT>2.0.CO;2

Wang, C., Deser, C., Yu, J.-Y., DiNezio, P., & Clement, A. (2017). El Niño and southern oscillation (ENSO): A review. In P. W. Glynn, D. P. Manzello, & I. C. Enochs (Eds.), *Coral reefs of the eastern tropical pacific* (Vol. 8, pp. 85–106). Springer. doi: 10.1007/978-94-017-7499-4_4

Wills, R. C. J., Dong, Y., Proistosecu, C., Armour, K. C., & Battisti, D. S. (2022). Systematic climate model biases in the large-scale patterns of recent sea-surface temperature and sea-level pressure change. *Geophysical Research Letters*, *49*(17), e2022GL100011. (Article e2022GL100011) doi: 10.1029/2022GL100011

Yokoi, S., Takayabu, Y. N., & Murakami, H. (2013, June 15). Attribution of projected future changes in tropical cyclone passage frequency over the Western North Pacific. *Journal of Climate*, *26*(12), 4096–4111. (Published: 15 June 2013) doi: 10.1175/JCLI-D-12-00218.1

Yoshida, K., Sugi, M., Mizuta, R., Murakami, H., & Ishii, M. (2017). Future changes in tropical cyclone activity in high-resolution large-ensemble simulations. *Geophysical Research Letters*, *44*(19), 9910–9917. doi: 10.1002/2017GL075058

Zarzycki, C. M., Jablonowski, C., & Taylor, M. A. (2014). Using variable-resolution meshes to model tropical cyclones in the Community Atmosphere Model. *Monthly Weather Review*, *142*, 1221–1239. doi: 10.1175/MWR-D-13-00179.1

Zhao, K., Zhao, H., Klotzbach, P. J., et al. (2026). Anthropogenic warming projected to drive a decline in global tropical cyclone frequency in CMIP6 simulations. *npj Climate and Atmospheric Science*, *9*, 58. (Article number 58) doi: 10.1038/s41612-026-01330-x

Zhuo, J. Y., Lee, C. Y., Sobel, A., Seager, R., Camargo, S. J., Lin, Y. H., … Reed, K. A. (2025). A more La Niña-like response to radiative forcing after flux adjustment in CESM2. *Journal of Climate*, *38*(4), 1037–1050. doi: 10.1175/JCLI-D-24-0331.1

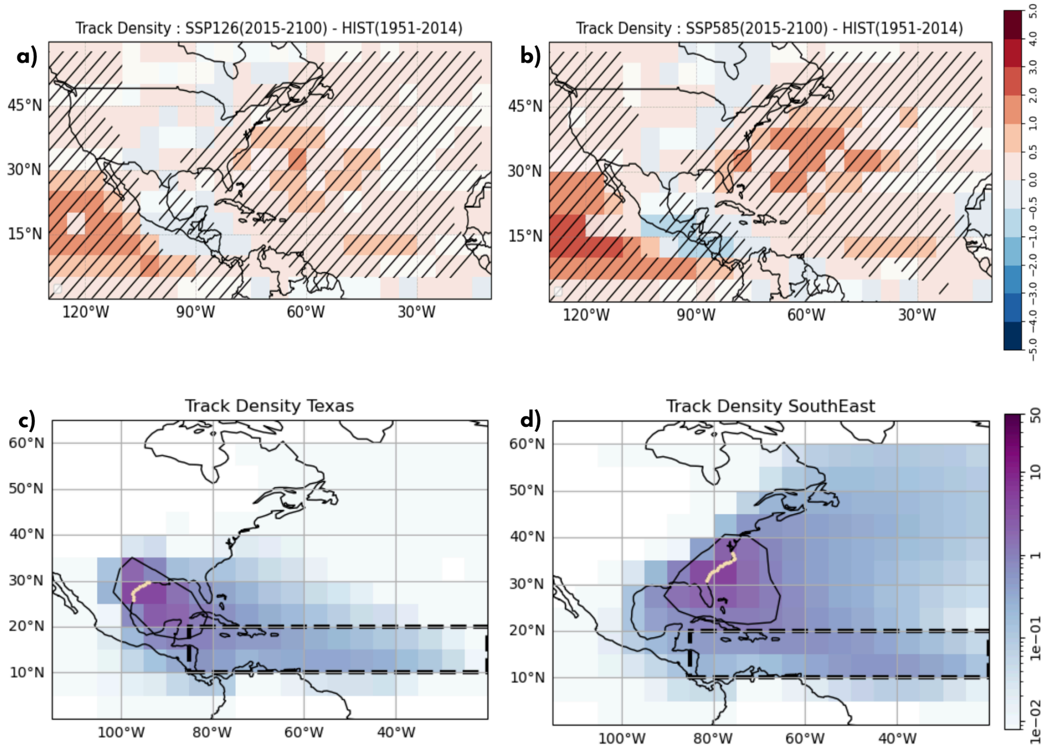

Figure 1: Multi-Model Mean of track density change in the North Atlantic, calculated between future and historical periods for SSP1-2.6 (a) and SSP5-8.5 (b). Stippling shows regions with statistically significant differences at $p = 0.05$ based on a two-sided Student's t-test from the 12-model, 10-track ensemble and 40-intensity ensemble. Average track density ($year^{-1}$) computed on a $5^o \times 5^o$ grid for tracks landfalling within the Texas (c) and Southeast (d) gates calculated for the historical period. The Atlantic MDR (dashed black), coastal gate (tan solid), and delineation for 1 storm per year (solid black contour) are shown for reference.

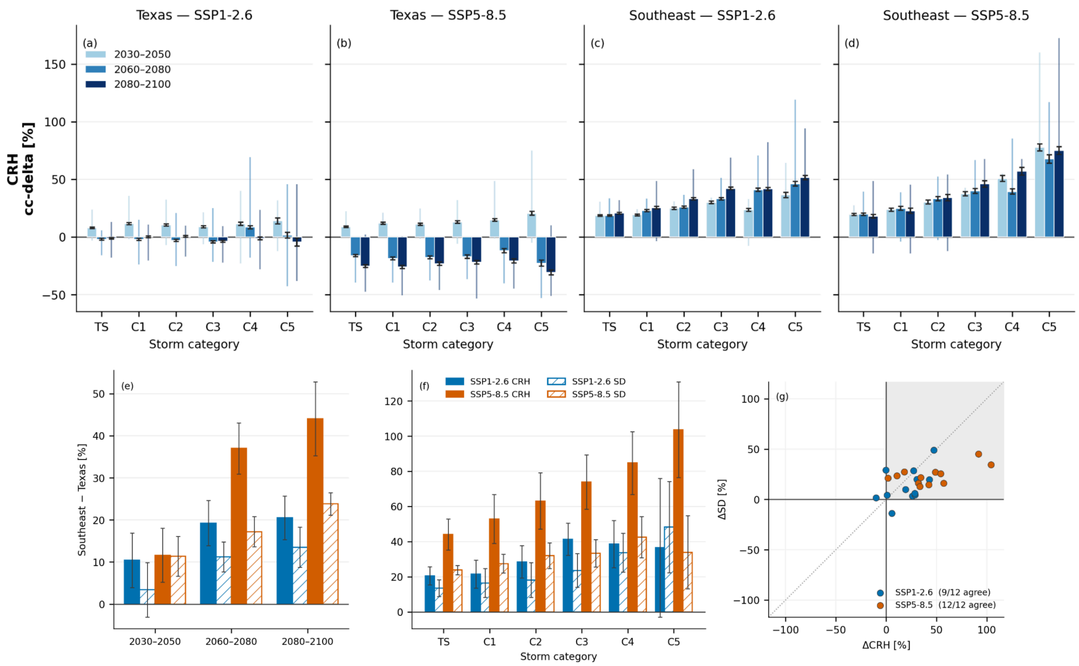

Figure 2: Change in TC frequency due to climate change (cc-delta) for SSP1-2.6 and SSP5-8.5 in the Texas (a,b) and Southeast gates (c,d) for near-term, mid-century and late century time periods from CHAZ CRH tracks (multi-model mean ± 95% confidence interval in black error bar, inter-quartile range in color stem). % difference in cc-delta between Southeast and Texas gates from CRH and SD CHAZ tracks in different future epochs (e), TC intensity categories (f), and within each of the 12-CMIP6 models (during 2080-2100) in the study (g).

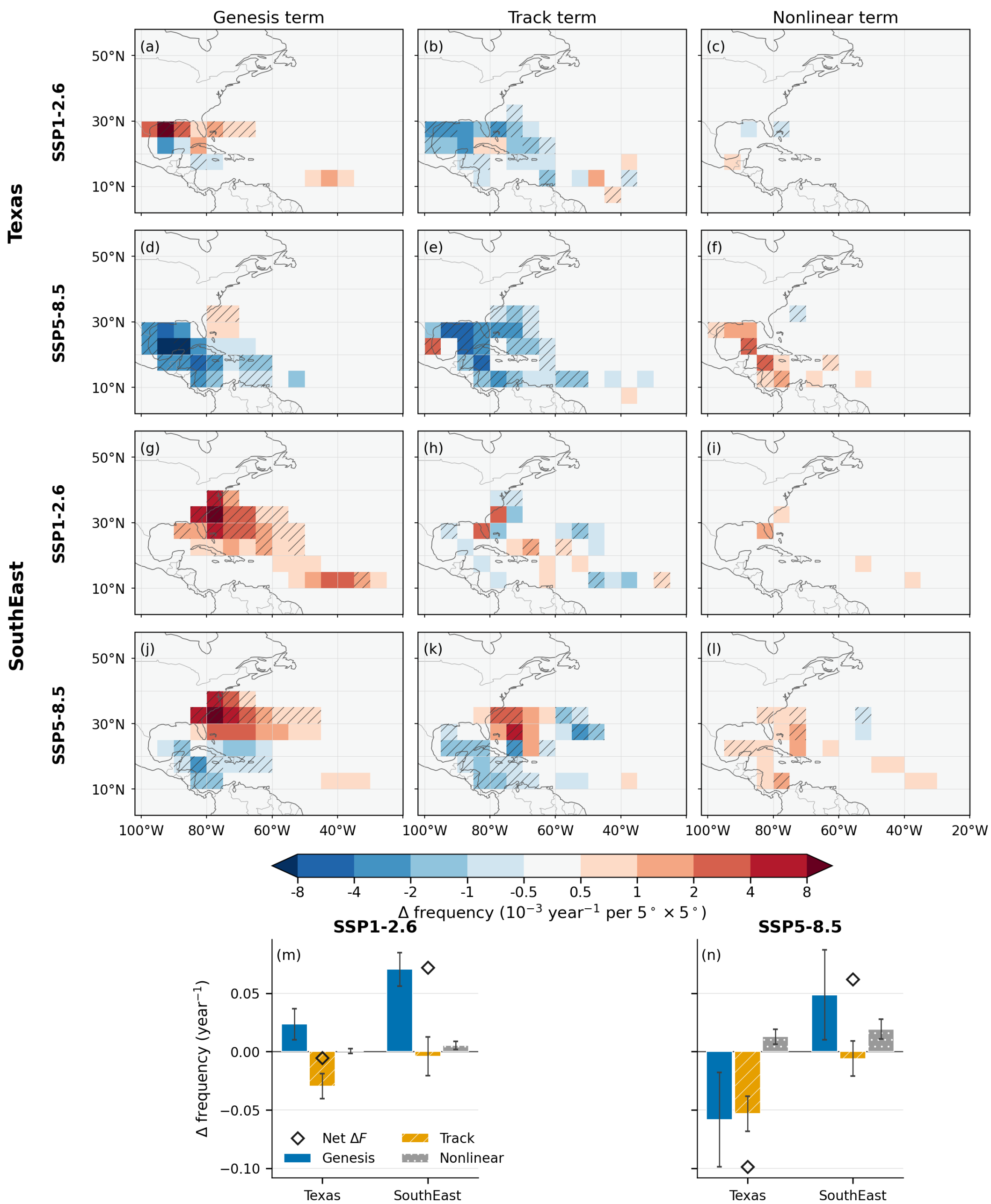

Figure 3: Origin analysis (Supporting Information Text S2) of the projected change in landfall frequency at the Texas (a–f) and Southeast (g–l) coastal gates for 2080–2100 relative to 1951–2014. Each cell shows the contribution of storms *originating* in that cell to the change in landfall frequency at the gate, so that summing a panel over all cells gives the corresponding bar in (m, n). Per-gate totals (m, n) from panels a–l for SSP1-2.6 and SSP5-8.5 genesis, track, nonlinear terms and the net frequency change, with error bars showing ±1 standard error across the 12 models. Hatching on the maps indicates cells where at least 75% of models agree on the sign of the plotted term. Contribution percentages quoted in the main text are these values normalized by the historical landfall frequency of the corresponding gate.

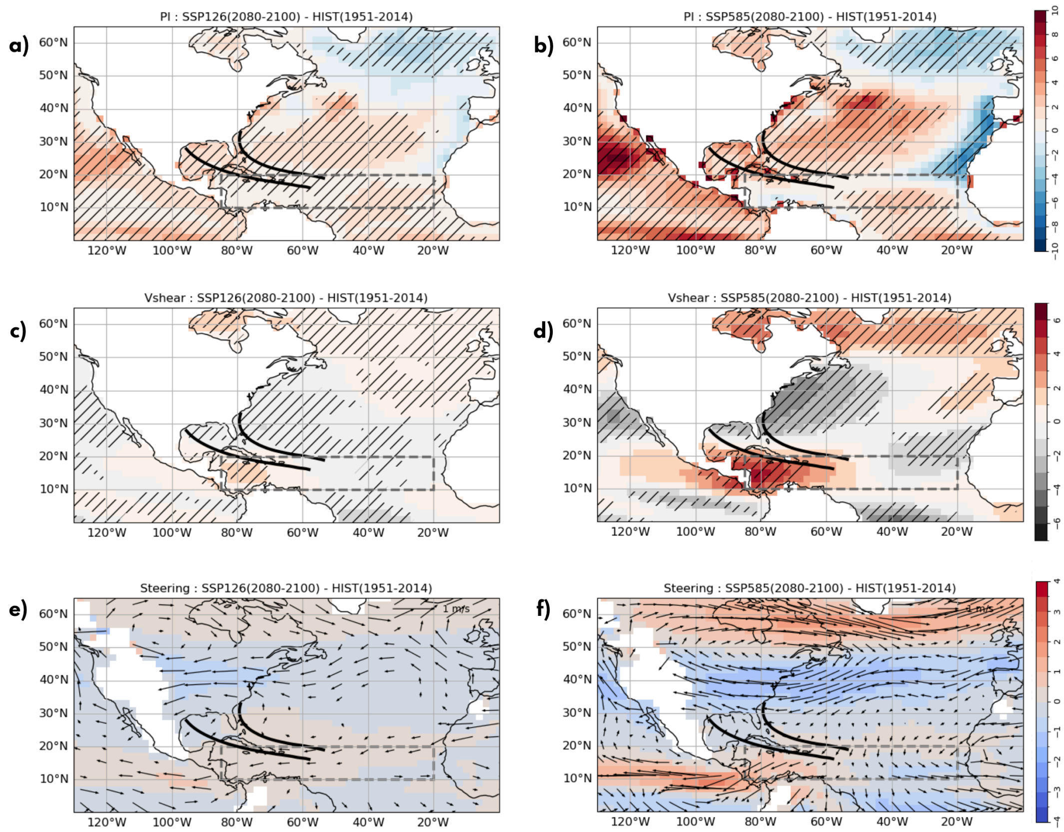

Figure 4: The multi-model mean difference between the late-century and historical period for PI change per degree of warming (dPI dT^{-1}) [a,b], 850-250 hPa vertical wind shear (m s^{-1}) [c,d], and mean steering flow (m s^{-1}) [e,f] for SSP1-2.6 and SSP5-8.5 (top and bottom respectively). Differences shown are calculated for August-October in the Northern Hemisphere. The average 10-day composite storm track for TCs landfalling within the Texas and Southeast gates, calculated 10 days prior to landfall using all storm tracks that made landfall within each gate (see Section 2.2) is also indicated (solid black), along with the Atlantic MDR (dashed black). Stippling indicates regions where at least 75% of models agree on the sign of the ensemble mean change.